Review of Scientific Instruments

RESEARCH ARTICLE | MAY 23 2023

Ultrafast electron diffraction instrument for gas and condensed matter samples

Yibo Wang ; Sajib Kumar Saha ; Tianlin Li ; Yanwei Xiong ; Kyle Wilkin ; Anil Adhikari ; Michael Loes ; Jehad Abourahma; Xia Hong ; Shireen Adenwalla ; Alexander Sinitskii ; Martin Centurion

Rev. Sci. Instrum. 94, 053001 (2023)
https://doi.org/10.1063/5.0146577

AIP Publishing

Review of Scientific Instruments ARTICLE scitation.org/journal/rsi

Ultrafast electron diffraction instrument for gas and condensed matter samples

Cite as: Rev. Sci. Instrum. 94, 053001 (2023); doi: 10.1063/5.0146577
Submitted: 15 February 2023 • Accepted: 4 May 2023 •
Published Online: 23 May 2023

Yibo Wang,[1,a] Sajib Kumar Saha,[1] Tianlin Li,[1] Yanwei Xiong,[1] Kyle Wilkin,[1] Anil Adhikari,[1] Michael Loes,[2] Jehad Abourahma,[2] Xia Hong,[1,3] Shireen Adenwalla,[1] Alexander Sinitskii,[2] and Martin Centurion[1,a]

AFFILIATIONS

[1] Department of Physics and Astronomy, University of Nebraska-Lincoln, 855 N 16th Street, Lincoln, Nebraska 68588-0298, USA
[2] Department of Chemistry, University of Nebraska-Lincoln, 855 N 16th Street, Lincoln, Nebraska 68588-0298, USA
[3] Nebraska Center for Materials and Nanoscience, University of Nebraska-Lincoln, Lincoln, Nebraska 65588-0298, USA

[a] **Authors to whom correspondence should be addressed:** yibo.wang@huskers.unl.edu and martin.centurion@unl.edu

ABSTRACT

We report the modification of a gas phase ultrafast electron diffraction (UED) instrument that enables experiments with both gas and condensed matter targets, where a time-resolved experiment with sub-picosecond resolution is demonstrated with solid state samples. The instrument relies on a hybrid DC-RF acceleration structure to deliver femtosecond electron pulses on the target, which is synchronized with femtosecond laser pulses. The laser pulses and electron pulses are used to excite the sample and to probe the structural dynamics, respectively. The new system is added with capabilities to perform transmission UED on thin solid samples. It allows for cooling samples to cryogenic temperatures and to carry out time-resolved measurements. We tested the cooling capability by recording diffraction patterns of temperature dependent charge density waves in 1T-TaS_2. The time-resolved capability is experimentally verified by capturing the dynamics in photoexcited single-crystal gold.

I. INTRODUCTION

Ultrafast laser pulses can create transient non-thermal states of matter, revealing new phenomena and mechanisms not accessible at the thermal equilibrium. Observing these states on their natural spatial and temporal scale requires a probe of Angstrom spatial resolution and femtosecond temporal resolution. Ultrafast electron diffraction (UED) captures, such ultrafast structural dynamics in terms of both the atomic nuclei and the electron system,[1,2] enabling further understanding of numerous physical and chemical phenomena that are associated with structural changes. UED has been applied successfully to study both condensed matter and gas phase systems. In the gas phase, UED has been a powerful tool to capture the structural dynamics of molecules.[3–8] With solid samples, UED has been used to study phase transitions and lattice dynamics in non-equilibrium states induced by femtosecond laser pulses.[1,2,9–11] Additionally, liquid phase UED experiments have recently become possible using relativistic electron beams and thin liquid sheets.[12]

In the past decade, there have been significant advances in UED instruments using both relativistic mega-electron-volt (MeV) electron sources[13–16] and table-top kilo-electron-volt (keV) DC guns.[1,8,9,17,18] For condensed matter applications, MeV electrons yield a large radius of the Ewald sphere, making it possible to observe diffraction orders with larger momentum transfer.

Previous UED instruments are designed and built to carry out experiments either with gas or solid samples and more recently also liquids. Changing the type of sample is in some cases not possible or requires replacing the target chamber. This is due to the different requirements for sample handling for gases, solids, and liquids. Swapping target chambers, which are designed for different sample types, require calibrations and diagnoses. Thus, it is time consuming and increases the overall cost of the instrument. Here, we report a keV UED setup that can carry out both gas phase and condensed matter experiments with a simple switch from the gas phase delivery system to the condensed matter sample holder, which can be done by accessing only one conflat vacuum flange.

II. SETUP DESCRIPTION

We have modified an existing gas phase UED instrument[8,19] to add the capability to carry out transmission UED experiments on condensed matter samples. Schematics of the UED beam lines are shown in Figs. 1 and 2. The key components of this experimental setup include a Ti:sapphire laser, a photoemission electron gun, an RF compressor and its timing system, a sample chamber, and an electron detector. The temporal profile of the electron pulses is characterized by a streak camera.[20]

Figure 1 shows a top view of the electron beam line. The ultrashort electron pulses are generated by photoemission in a photocathode illuminated by femtosecond UV laser pulses. The UV laser pulses are directed to the center of the photocathode by an in-vacuum UV mirror, and the reflected laser beam is monitored for adjusting beam pointing. The generated electron pulses are accelerated by a 90 kV electrostatic field. After the electron beam traverses a small aperture in the anode, its steering and transverse divergence are controlled through two magnetic deflectors and two magnetic lenses, respectively. An RF cavity with a time-variant electric field is used to compress the electron pulses longitudinally, with the temporal focus downstream at the sample position. In the sample chamber, platinum pinholes of different sizes are mounted on an actuated collimator, reducing the beam size and cutting off diffused electrons. An actuated vacuum flange on top of the sample chamber can be mounted with a gas nozzle or a cold finger for experiments in the gas and solid phase, respectively. After interacting with the sample in the gas or solid phase, the diffracted electron beam is captured with a phosphor screen, which is imaged onto an EMCCD camera. A compact six-way cube connects the exit of the sample chamber and the phosphor screen. The small distance between the screen and sample allows a large momentum transfer range of 12.5 inverse Angstrom from the center of the detector to its edge, which roughly corresponds to 20 inverse nanometers in reciprocal space units, as commonly used in transmission electron microscopy (TEM). A motion controlled Faraday cup between the sample and phosphor screen measures the current of the transmitted electron beam and prevents it from getting to the camera, providing an increased dynamic range for the diffraction images.

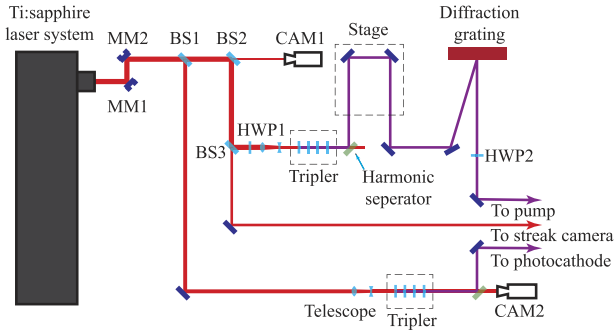

FIG. 2. A sketch of the optical setup showing the three beam paths. A beam pointing stabilization system consisting of two motorized mirrors (MM1 and MM2) and two cameras (CAM1 and CAM2) is set after the exit of the laser amplifier. Beam splitters (BS1, BS2, and BS3) divide the beam into three main branches: to pump the sample, to trigger the streak camera, and to excite the photocathode. A diffraction grating after the delay stage creates a tilted energy front in the pump pulse.

A. The optical setup

The setup begins with a Ti:sapphire laser system, consisting of a mode-locked oscillator and a chirped-pulse amplifier. The oscillator generates seed laser pulses of 800 nm central wavelength at a repetition rate of 75 MHz. Such repetition rate is stabilized by controlling the cavity length with one end mirror on a fine motion stage. The amplifier outputs 1.7 mJ, 40 fs pulses of 800 nm central wavelength with a bandwidth of 60 nm at up to 5 kHz repetition rate. Figure 2 illustrates the optical setup. After the laser pulses exit the laser amplifier, a pair of motorized mirrors are placed in the beam line to adjust the laser beam direction and positioning according to the feedback from two CCD cameras to minimize the variations in the beam pointing. The laser beam is then divided into three branches: I. to generate the electron probe beam; II. to pump the sample; and III. to trigger an electron streaking device.

For branch I, a small portion of the laser beam is harmonically tripled to a UV wavelength. After the UV beam is focused by

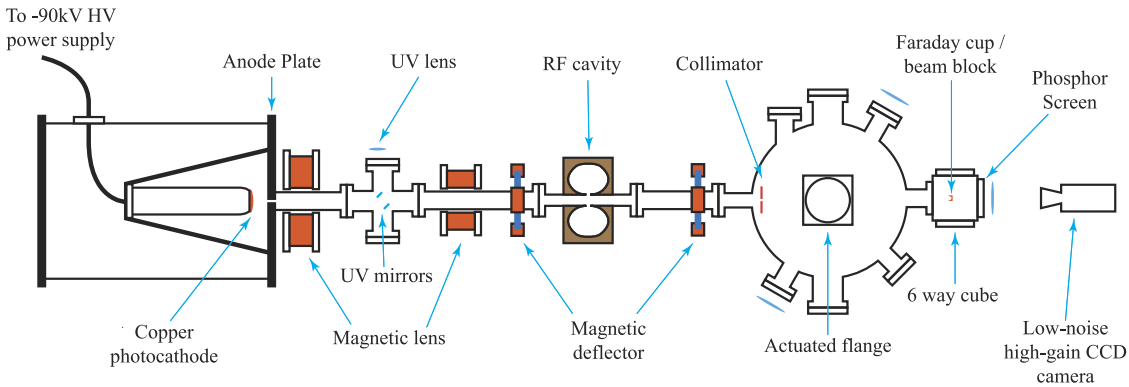

FIG. 1. Schematic representation of the electron beam line of the UED setup. Home-made electron optics include two magnetic lenses and two deflectors that are used to focus the electron beam and guide the electron beam, respectively. An RF cavity compresses the electron beam longitudinally, with a temporal focus at the sample's location.

a UV lens outside the vacuum, an in-vacuum UV mirror directs the beam to the center of the photocathode, and the reflected UV beam is captured by a UV camera to ensure optimal beam pointing on the photocathode. A neutral density filter wheel is deployed in this beam path to adjust the pulse energy of the UV pulses, which controls the charge of the electron pulses.

Laser branch II is used to excite the sample, which contains most of the energy of the laser beam. A mechanical delay stage is used to match the time of arrival of the pump laser pulse and the electron pulse on the sample. The pump beam is delivered to the sample at an incident angle of around 60° so that the velocity components of both beams along the direction of propagation of the electron beam are matched. The pulse front of the laser is tilted using a plane ruled gold reflection grating and an imaging system such that it is parallel to the electron intensity front at the sample.[21] For gas phase experiments, the tilted laser pulse ensures that there is no velocity mismatch as the beams traverse the sample; for thin condensed matter samples where velocity mismatch is not an issue, the tilted pulse illuminates the whole sample simultaneously. The intensity of the pump excitation is controlled with a half wave plate and a polarizing beam splitter, combined with a neutral density filter wheel. The pump laser beam at the sample position is imaged to a CCD camera to determine the spatial overlap of the laser and the sample.

Laser branch III is used to trigger the electron streak camera, details of which have been published previously.[20]

B. The radio frequency electron beam compression

The Coulomb expansion of the electron pulse poses the main challenge for the temporal resolution of UED experiments. One method to compensate for the Coulomb expansion is electron pulse compression through an RF cavity.[9,22–23] We place the RF cavity at a distance of 580 mm from the photocathode and 220 mm from the sample. As the electron pulse traverses the RF cavity, the electrons in the leading edge are decelerated, and electrons in the trailing edge are accelerated by the time varying electric field in the cavity. This results in a temporal focus of the electron pulse downstream of the cavity, at the sample position. We built a custom stabilization and synchronization system to stabilize the phase and timing of the time-varying electric field in the RF cavity,[19] based on prior work by the Siwick group.[24]

C. The cold finger and sample holder

The sample chamber houses a mechanical 3D actuator on top, on which either a flange connecting the gas nozzle or a cold finger attached to the sample holder for samples in solid phase can be placed. In order to modify the setup from the gas phase to solid samples, the flange carrying the gas delivery system is replaced by a homemade cold finger, whose half section diagram is shown in Fig. 3(a). The main body of the cold finger is a four-way cross attached below a custom reducer flange that houses a rotary feedthrough and a pair of inlet and outlet tubes for the liquid nitrogen reservoir. One side flange of the four-way cross houses thermocouple feedthrough. The bottom flange of this four-way cross connects to the top of the 3D actuator above the sample chamber.

The rotary feedthrough at the top of the cold finger gives an additional rotation degree of freedom to the sample orientation. An adjustable angle between the sample surface and the probing electron beam allows optimizing for different Bragg conditions.[25] In addition, the stacking order of the single crystal specimen in the z direction can be examined when the probe and the normal direction of the specimen are at a small angle.[26]

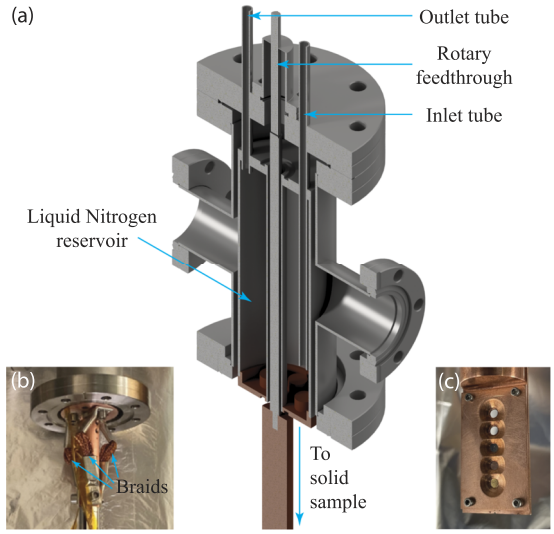

FIG. 3. (a) A cross-sectional diagram of the main body of the cold finger. In vacuum, a hollow cylinder liquid nitrogen reservoir sits at the center of a conflat four-way reducing cross (4.5 in. OD vertical and 2.5 in. OD horizontal). The reservoir connects to the air through inlet and outlet tubes on top. A rotary feed through is connected to a stainless steel rod that goes through the center axis of the liquid nitrogen reservoir to provide rotary motion to the sample. (b) A photograph of the bottom of the liquid nitrogen reservoir. Three copper braids provide thermal conduction between the bottom of the liquid nitrogen reservoir and the copper rod while allowing the rod to rotate at the same time. Everything between the liquid nitrogen and the sample is made of copper. Thermal grease and silver paste are applied at selective points for the best thermal conductivity. (c) The copper sample holder with samples mounted. When mounting a sample grid, the cover piece and the base piece sandwich the sample grid in the center slot. The tapered sample slots give clearance to the laser beam incident from a 60° angle.

The stainless steel inlet and outlet tubes connect and support the liquid nitrogen reservoir, which takes the shape of a cylinder and fills up most of the space inside the four-way cross with a small gap between the outer wall of the reservoir and the inner wall of the four-way cross. The rod connecting the rotary feedthrough and the sample holder passes through a hole in the center of the reservoir. Figure 3(b) shows the connection between the reservoir and the rod. For the best thermal conductivity, the bottom piece of the reservoir is made of oxygen free copper and thermally connected to the central copper rod through three braided copper wires.

The solid phase samples are mounted on metal and thin organic film based TEM sample grids or semiconductor based membranes. The TEM grids with 3 mm diameter are mounted on a custom made sample holder made of oxygen free copper at the bottom of the cold finger. As shown in Fig. 3, the slots that hold the TEM grids are reverse tapered with an angle of −75° to give clearance to the incoming and exiting laser beam. We tested the cooling capabilities of the cold finger. It can cool the sample from room temperature to 90 K in 80 min and reach thermal equilibrium at such temperature.

III. TEMPERATURE DEPENDENT CDW

We demonstrate the cooling ability of this cold finger by comparing diffraction patterns of 1T-TaS_2 at room temperature and 90 K. TaS_2 is a two dimensional semiconductor that, in octahedrally coordinated polytype, exhibits a charge density wave at temperatures below 550 K. It transitions to a near-commensurate charge density wave (NCCDW) phase below 350 K and to a commensurate charge density wave (CCDW) phase below around 180 K.[27] Due to the presence of a charge density wave, at NCCDW and CCDW phases, the thin TaS_2 sample experiences a periodic lattice distortion, which generates a superlattice pattern that forms domains across the sample. Such superlattice of higher order symmetry is reflected in the electron diffraction pattern as satellite diffraction spots in addition to the Bragg diffraction orders. Previous UED studies have shown the ultrafast structural dynamics of the charge density wave system after optical excitation.[26,28–31]

In this work, thin TaS_2 flakes (bulk 1T-TaS_2 from HQ graphene®) are mechanically exfoliated using the Scotch tape method onto a silicone gel film (Gel-Film® PF-40-X4 from Gel-Pak). Sample flakes whose thickness is in the range of tens of nanometers are identified optically before being transferred onto formvar covered TEM grids via standard high-temperature dry transfer technique.[32,33] An actuated transfer stage has been adapted for horizontal alignment and fine vertical adjustments. The selected TaS_2 flake is kept aligned to the desired location as the gel film approaches the TEM grid. After the gel film contacts the TEM grid, gentle pressure is applied, and the transfer stage is heated to 80 °C for 300 s for better adhesion. Then, the gel film is gently released from the TEM grid, with the desired sample flake attached to the TEM grid.

The electron diffraction patterns are taken from a TaS_2 sample whose lateral size is ~40 μm. In order to maintain a reasonable signal to noise ratio, a titanium pinhole of 30 μm diameter is placed in the electron beam path. At a cost of reduced beam current, a smaller electron beam matches the sample size and creates a smaller spot size on the screen, improving the momentum resolution and giving clearer satellite diffraction peaks.

We see significant differences between the diffraction patterns of the TaS_2 at room temperature and at 90 K (Fig. 4). The intensity of all Laue diffraction orders increases when the temperature is reduced to 90 K, as would be expected from the lowered lattice vibrations. For the satellite diffraction orders, the intensity and the number of distinguishable orders increase, suggesting an increased domain size of the CDW covered surface area on the sample as a result of the transition to the commensurate phase of charge density wave. The presented diffraction approach should be also applicable to studies of many other layered CDW materials.[34]

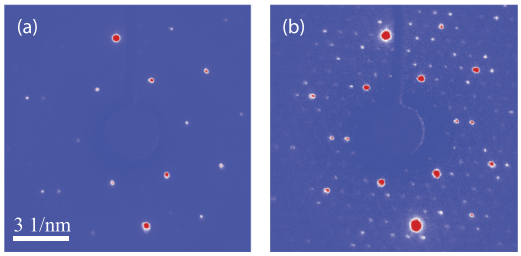

FIG. 4. (a) and (b) Electron diffraction patterns of TaS_2 sample at room temperature and 90 K, respectively. More CDW diffraction orders become visible at cold temperatures.

IV. A TIME-RESOLVED EXPERIMENT

A time-resolved experiment is performed on a single crystal gold film to validate the full UED capacity of the experimental setup. To carry out pump–probe experiments, we first need to find the temporal overlap of the laser (pump) and electron (probe) pulses. We find this time zero by shining the laser pulses on a metal surface to create a cloud of photoelectrons. This process produces electromagnetic fields that distort the electron beam.[35]

A. Temporal overlap

To achieve the temporal overlap of the pump and probe beams, we take advantage of the single- or multi-photon photoemission process of a copper knife edge on the sample holder. Figure 5(a) sketches the mechanism of the time-resolved electron beam distortion: after the pump of 267 nm wavelength and 40 mJ/cm^2 fluence, the copper knife edge emits a cloud of charge. The electric field generated by the photoemmited electrons deflects the electron pulse toward the copper knife edge.

After the pump and probe beams are spatially aligned to the same spot on the knife edge of the sample holder, images of the electron beam near the knife edge are taken repeatedly at different delay positions. Figure 5(c) shows the difference in images with electrons

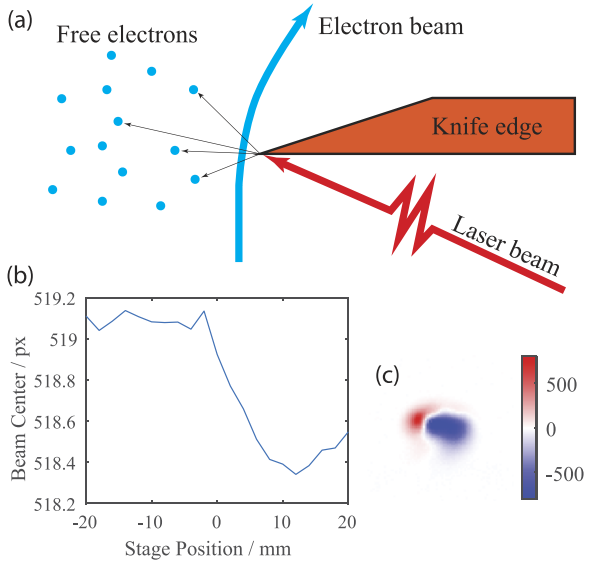

FIG. 5. (a) A top-view diagram of the setup to determine the temporal overlap of laser and electron pulses. Free electrons are generated by the photo-ionization of a copper knife edge. The electron beam is deflected by the fields produced after photoemission. (b) The response of the horizontal position of the electron beam to the time delay between the laser and electron pulses (presented by the delay stage position). (c) A differential image of the electron beam before and 6.7 ps after time zero, where the electron beam is deflected toward the left side of the screen.

arriving after the laser and before the laser. The deflection of the electron beam shows a clear time dependence which can be used to determine the time zero. Figure 5(b) shows the measured deflection vs time, where the time zero is marked by the stage position where the horizontal shift starts.

B. Time-resolved electron diffraction of gold

In the time-resolved ultrafast heating experiment, the sample is a single crystal gold film of 30 nm thickness attached to a gold TEM grid (Rave Scientific EM-Tec TC1). The pump laser has a wavelength of 267 nm, a 1 kHz repetition rate, and a 150 μm diameter on the sample. As Fig. 6 shows, after the laser excitation, the intensity of the diffraction orders decreases rapidly while the diffuse scattering between the Bragg peaks increases. Taking a closer look at the dynamics in different orders of Bragg diffraction, we averaged the dynamics of the {022} orders of similar symmetry, which are at the same momentum transfer range, along with the dynamics of the diffuse scatterings. The latter is characterized by averaging a ring in the diffraction pattern within the four lowest order diffraction spots. The results are plotted in Fig. 7. For all of the Bragg diffraction orders, the suppression of the intensities happens on a time scale of 3–5 ps, and the diffuse scattering increases on a similar time scale. These are the results of an ultrafast nonthermal heating of the gold lattice.

The UV pump interacts directly with the carrier system. The absorption of photons leads to an ultrafast population of hot carriers that reach thermal equilibrium among themselves through electron-electron scattering and carrier diffusion on a time scale of less than a hundred femtoseconds. In order to reach thermal equilibrium with the relatively cold lattice system, the carriers lose energy via carrier–phonon interaction. The lattice temperature continues to rise during this process, which lasts a few picoseconds until the carrier system and lattice system reach thermal equilibrium. This corresponds to the decrease in the intensity of the diffraction spots. After the intensity of the Bragg diffraction orders reaches the minimum, it starts to slowly recover. Thermal relaxation of the two subsystems due to thermal diffusion of the lattice and heat exchange with the substrate takes place on a longer time scale of hundreds of picoseconds. These results agree with prior experiments of the ultrafast heating[36–37] and melting[38–40] of gold.

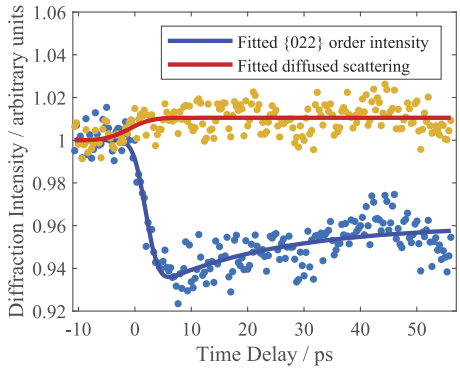

FIG. 7. Time resolved diffraction intensity of the {022} diffraction orders and the diffuse scatterings of single crystalline gold. The suppression of the intensities due to the lattice heating is on a time scale of 3 ps. The rise of diffuse scatterings is on a similar time scale.

These time-resolved signals have clearly demonstrated the capability of this UED setup in solid phase experiments.

V. CONCLUSION

In conclusion, we demonstrate a keV table-top UED instrument for studying samples in a solid state and the gas phase. With the home made cold finger, samples in the solid state can be reliably cooled to cryo temperatures. The system has good temporal and momentum resolution with high electron beam brightness and can be operated in different repetition rates up to 5 kHz.

The cooling is demonstrated by capturing the phase transition in TaS_2 from NCCDW to CCDW, which shows clear changes in the electron diffraction patterns. The time resolution was demonstrated with a time-resolved pump–probe experiment on a single crystal thin gold film. The reduction in the diffraction intensities due to lattice heating was captured with sub-picosecond resolution.

ACKNOWLEDGMENTS

This work was supported by the National Science Foundation through EPSCoR RII Track-1: Emergent Quantum Materials

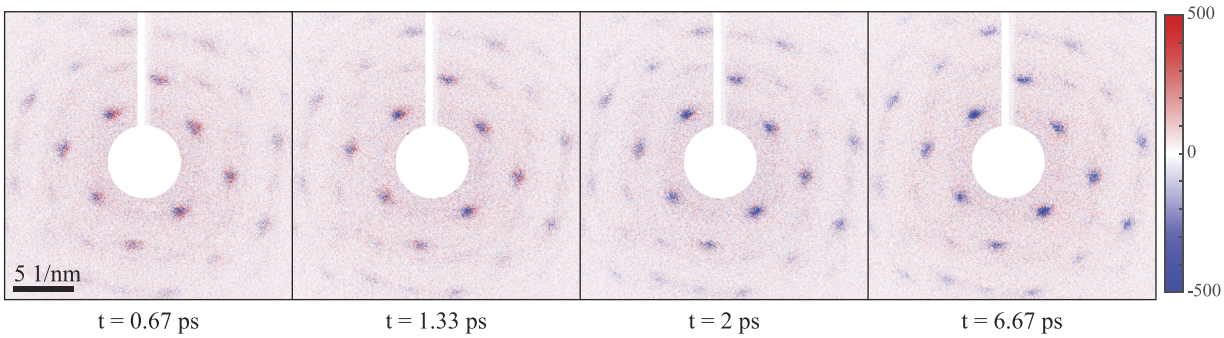

FIG. 6. A series of diffraction patterns of the single crystal gold sheet at different time delays, subtracting the diffraction pattern before time zero.

and Technologies (EQUATE) under Award No. OIA-2044049, and the Nebraska Research Initiative Collaboration Seed under Grant No. 21-0521. The research was performed in part in the Nebraska Nanoscale Facility: National Nanotechnology Coordinated Infrastructure and the Nebraska Center for Materials and Nanoscience, which are supported by the National Science Foundation under Award No. ECCS: 2025298, and the Nebraska Research Initiative.

AUTHOR DECLARATIONS

Conflict of Interest

The authors have no conflicts to disclose.

Author Contributions

Yibo Wang: Conceptualization (equal); Data curation (equal); Formal analysis (equal); Investigation (equal); Methodology (equal); Writing – original draft (equal). **Sajib Kumar Saha**: Data curation (supporting); Methodology (supporting). **Tianlin Li**: Methodology (supporting); Writing – original draft (supporting). **Yanwei Xiong**: Methodology (supporting); Writing – review & editing (supporting). **Kyle Wilkin**: Methodology (supporting). **Anil Adhikari**: Methodology (supporting). **Michael Loes**: Methodology (supporting). **Jehad Abourahma**: Methodology (supporting). **Xia Hong**: Funding acquisition (supporting); Methodology (supporting); Resources (supporting); Supervision (supporting); Validation (supporting); Writing – review & editing (supporting). **Shireen Adenwalla**: Conceptualization (supporting); Funding acquisition (supporting); Methodology (supporting); Resources (supporting); Supervision (supporting); Validation (supporting); Writing – review & editing (supporting). **Alexander Sinitskii**: Conceptualization (supporting); Resources (supporting); Supervision (supporting). **Martin Centurion**: Conceptualization (equal); Formal analysis (equal); Funding acquisition (equal); Investigation (equal); Methodology (equal); Project administration (equal); Resources (equal); Supervision (equal); Validation (equal); Writing – review & editing (equal).

DATA AVAILABILITY

The data that support the findings of this study are available from the corresponding authors upon reasonable request.

REFERENCES

[1]B. J. Siwick, J. R. Dwyer, R. E. Jordan, and R. J. D. Miller, Science **302**, 1382 (2003).
[2]G. Sciaini and R. J. D. Miller, Rep. Prog. Phys. **74**, 096101 (2011).
[3]R. Srinivasan, V. A. Lobastov, C.-Y. Ruan, and A. H. Zewail, Helv. Chim. Acta **86**, 1761 (2003).
[4]P. Reckenthaeler, M. Centurion, W. Fuß, S. A. Trushin, F. Krausz, and E. E. Fill, Phys. Rev. Lett. **102**, 213001 (2009).
[5]C. J. Hensley, J. Yang, and M. Centurion, Phys. Rev. Lett. **109**, 133202 (2012).
[6]J. Yang, M. Guehr, T. Vecchione, M. S. Robinson, R. Li, N. Hartmann, X. Shen, R. Coffee, J. Corbett, A. Fry, K. Gaffney, T. Gorkhover, C. Hast, K. Jobe, I. Makasyuk, A. Reid, J. Robinson, S. Vetter, F. Wang, S. Weathersby, C. Yoneda, X. Wang, and M. Centurion, Faraday Discuss. **194**, 563 (2016).
[7]X. Shen, J. P. F. Nunes, J. Yang, R. K. Jobe, R. K. Li, M.-F. Lin, B. Moore, M. Niebuhr, S. P. Weathersby, T. J. A. Wolf, C. Yoneda, M. Guehr, M. Centurion, and X. J. Wang, Struct. Dyn. **6**, 054305 (2019).
[8]O. Zandi, K. J. Wilkin, Y. Xiong, and M. Centurion, Struct. Dyn. **4**, 044022 (2017).
[9]T. van Oudheusden, P. L. E. M. Pasmans, S. B. van der Geer, M. J. de Loos, M. J. van der Wiel, and O. J. Luiten, Phys. Rev. Lett. **105**, 264801 (2010).
[10]V. R. Morrison, R. P. Chatelain, K. L. Tiwari, A. Hendaoui, A. Bruhács, M. Chaker, and B. J. Siwick, Science **346**, 445 (2014).
[11]M. Gao, C. Lu, H. Jean-Ruel, L. C. Liu, A. Marx, K. Onda, S.-y. Koshihara, Y. Nakano, X. Shao, T. Hiramatsu, G. Saito, H. Yamochi, R. R. Cooney, G. Moriena, G. Sciaini, and R. J. D. Miller, Nature **496**, 343 (2013).
[12]J. P. F. Nunes, K. Ledbetter, M. Lin, M. Kozina, D. P. DePonte, E. Biasin, M. Centurion, C. J. Crissman, M. Dunning, S. Guillet, K. Jobe, Y. Liu, M. Mo, X. Shen, R. Sublett, S. Weathersby, C. Yoneda, T. J. A. Wolf, J. Yang, A. A. Cordones, and X. J. Wang, Struct. Dyn. **7**, 024301 (2020).
[13]R. Li, C. Tang, Y. Du, W. Huang, Q. Du, J. Shi, L. Yan, and X. Wang, Rev. Sci. Instrum. **80**, 083303 (2009).
[14]S. P. Weathersby, G. Brown, M. Centurion, T. F. Chase, R. Coffee, J. Corbett, J. P. Eichner, J. C. Frisch, A. R. Fry, M. Gühr, N. Hartmann, C. Hast, R. Hettel, R. K. Jobe, E. N. Jongewaard, J. R. Lewandowski, R. K. Li, A. M. Lindenberg, I. Makasyuk, J. E. May, D. McCormick, M. N. Nguyen, A. H. Reid, X. Shen, K. Sokolowski-Tinten, T. Vecchione, S. L. Vetter, J. Wu, J. Yang, H. A. Dürr, and X. J. Wang, Rev. Sci. Instrum. **86**, 073702 (2015).
[15]F. Fu, S. Liu, P. Zhu, D. Xiang, J. Zhang, and J. Cao, Rev. Sci. Instrum. **85**, 083701 (2014).
[16]H. W. Kim, N. A. Vinokurov, I. H. Baek, K. Y. Oang, M. H. Kim, Y. C. Kim, K.-H. Jang, K. Lee, S. H. Park, S. Park, J. Shin, J. Kim, F. Rotermund, S. Cho, T. Feurer, and Y. U. Jeong, Nat. Photonics **14**, 245 (2020).
[17]T. LaGrange, B. W. Reed, M. K. Santala, J. T. McKeown, A. Kulovits, J. M. K. Wiezorek, L. Nikolova, F. Rosei, B. J. Siwick, and G. H. Campbell, Micron **43**, 1108 (2012), *in situ* TEM.
[18]W. H. Li, C. J. R. Duncan, M. B. Andorf, A. C. Bartnik, E. Bianco, L. Cultrera, A. Galdi, M. Gordon, M. Kaemingk, C. A. Pennington, L. F. Kourkoutis, I. V. Bazarov, and J. M. Maxson, Struct. Dyn. **9**, 024302 (2022).
[19]Y. Xiong, K. J. Wilkin, and M. Centurion, Phys. Rev. Res. **2**, 043064 (2020).
[20]O. Zandi, K. J. Wilkin, and M. Centurion, Rev. Sci. Instrum. **88**, 063305 (2017).
[21]P. Zhang, J. Yang, and M. Centurion, New J. Phys. **16**, 083008 (2014).
[22]R. P. Chatelain, V. R. Morrison, C. Godbout, and B. J. Siwick, Appl. Phys. Lett. **101**, 081901 (2012).
[23]T. van Oudheusden, E. F. de Jong, S. B. van der Geer, W. P. E. M. O. 't Root, O. J. Luiten, and B. J. Siwick, J. Appl. Phys. **102**, 093501 (2007).
[24]M. R. Otto, L. P. René de Cotret, M. J. Stern, and B. J. Siwick, Struct. Dyn. **4**, 051101 (2017).
[25]I. González Vallejo, G. Gallé, B. Arnaud, S. A. Scott, M. G. Lagally, D. Boschetto, P.-E. Coulon, G. Rizza, F. Houdellier, D. Le Bolloc'h, and J. Faure, Phys. Rev. B **97**, 054302 (2018).
[26]L. Le Guyader, T. Chase, A. H. Reid, R. K. Li, D. Svetin, X. Shen, T. Vecchione, X. J. Wang, D. Mihailovic, and H. A. Dürr, Struct. Dyn. **4**, 044020 (2017).
[27]A. Spijkerman, J. L. de Boer, A. Meetsma, G. A. Wiegers, and S. van Smaalen, Phys. Rev. B **56**, 13757 (1997).
[28]M. Eichberger, H. Schäfer, M. Krumova, M. Beyer, J. Demsar, H. Berger, G. Moriena, G. Sciaini, and R. J. D. Miller, Nature **468**, 799 (2010).
[29]T.-R. T. Han, F. Zhou, C. D. Malliakas, P. M. Duxbury, S. D. Mahanti, M. G. Kanatzidis, and C.-Y. Ruan, Sci. Adv. **1**, e1400173 (2015).
[30]K. Haupt, M. Eichberger, N. Erasmus, A. Rohwer, J. Demsar, K. Rossnagel, and H. Schwoerer, Phys. Rev. Lett. **116**, 016402 (2016).
[31]P. Zhu, Y. Zhu, Y. Hidaka, L. Wu, J. Cao, H. Berger, J. Geck, R. Kraus, S. Pjerov, Y. Shen, R. I. Tobey, J. P. Hill, and X. J. Wang, New J. Phys. **17**, 063004 (2015).
[32]Y. Liang, J. Zhu, F. Xiao, B. Xu, T. Wen, S. Wu, J. Li, J. Xia, and Z. Wang, IEEE J. Electron Devices Soc. **9**, 1269 (2021).
[33]Y.-Q. Bie, A. Zong, X. Wang, P. Jarillo-Herrero, and N. Gedik, Ultramicroscopy **230**, 113389 (2021).

[34]M. D. Randle, A. Lipatov, I. Mansaray, J. E. Han, A. Sinitskii, and J. P. Bird, Appl. Phys. Lett. **118**, 210502 (2021).
[35]H. Park, Z. Hao, X. Wang, S. Nie, R. Clinite, and J. Cao, Rev. Sci. Instrum. **76**, 083905 (2005).
[36]M. Ligges, I. Rajkovic, P. Zhou, O. Posth, C. Hassel, G. Dumpich, and D. von der Linde, Appl. Phys. Lett. **94**, 101910 (2009).
[37]S. Schäfer, W. Liang, and A. H. Zewail, Chem. Phys. Lett. **515**, 278 (2011).
[38]R. Ernstorfer, M. Harb, C. T. Hebeisen, G. Sciaini, T. Dartigalongue, and R. J. D. Miller, Science **323**, 1033 (2009).
[39]P. Musumeci, J. T. Moody, C. M. Scoby, M. S. Gutierrez, and M. Westfall, Appl. Phys. Lett. **97**, 063502 (2010).
[40]M. Z. Mo, Z. Chen, R. K. Li, M. Dunning, B. B. L. Witte, J. K. Baldwin, L. B. Fletcher, J. B. Kim, A. Ng, R. Redmer, A. H. Reid, P. Shekhar, X. Z. Shen, M. Shen, K. Sokolowski-Tinten, Y. Y. Tsui, Y. Q. Wang, Q. Zheng, X. J. Wang, and S. H. Glenzer, Science **360**, 1451 (2018).